scientific reports

Check for updates

OPEN

Bio-nanoparticles sensor couple with smartphone digital image colorimetry and dispersive liquid–liquid microextraction for aflatoxin B1 detection

Mahsa Alikord[1,2]✉, Nabi Shariatifar[3]✉, Mammad Saraji[4], Hedayat Hosseini[5], Gholamreza Jahed Khaniki[3], Shahram Shoeibi[6], Toba Rezazadeh[4] & Mohammad Fazeli[7]

A novel nanobiosensor-based colorimetric method was developed by integrating ZnO nanoparticles functionalized with curcumin, dispersive liquid–liquid microextraction (DLLME), and smartphone digital image colorimetry for the sensitive detection of aflatoxin B1 (AFB1) in baby food samples. The unique combination of biologically-derived ZnO nanoparticles with curcumin created a sensing platform, while DLLME provided efficient pre-concentration of the target analyte. A custom-designed portable colorimetric box enabled standardized image capture and analysis using a smartphone camera and colorimetric software. Under optimized conditions using chloroform as the extraction solvent and acetonitrile as the disperser solvent, the method achieved a remarkable limit of detection of 0.09 µg/kg within linear concentration range of 0–1 µg/L. The calibration curves demonstrated excellent linearity ($R^2 > 0.9906$) with high precision (RSD < 5.52%). The method was successfully validated using baby food samples, achieving high recoveries (89.8–94.2%). This innovative integration of nanobiosensing, microextraction, and smartphone technology offers a rapid, highly sensitive, and cost-effective platform for on-site AFB1 detection in food safety applications, particularly beneficial for resource-limited settings.

Keywords Smartphone detection, Curcumin, Zinc oxide nanoparticles, Aflatoxin B1, Baby food, Dispersive liquid–liquid microextraction

Mycotoxins, secondary metabolites produced by fungi under specific temperature and humidity conditions, can contaminate various kinds of foods such as oilseeds, crops, milk, meat, eggs, etc. Aflatoxins (AFs), classified as Group 1 carcinogens by IARC, are primarily produced by *Aspergillus flavus*, *A. parasiticus*, and *A. nomius*. Specifically, *A. flavus* produces aflatoxin B (AFB1 and AFB2), whereas *A. parasiticus* and *A. nomius* produce both aflatoxin B (AFB1 and AFB2) and aflatoxin G (AFG1 and AFG2)[1]. Exposure to AFs through foods is a significant threat to animal and human health. The integration of multiple grains and crops in infant formula and baby food increases the chances of contamination with various mycotoxins in sensitive and vulnerable groups. Global contamination rates in baby foods range from 20 to 60%, presenting a significant threat to infant health[2]. Thus, monitoring studies are essential to determine the levels of aflatoxin contamination. Conspicuously, the European Union has set the strictest levels for aflatoxin B1 (0.1 µg/kg) in infant and baby foods, as outlined in Commission Regulations (EC) No 1881/2006. However, there is currently no maximum limit established for total aflatoxins (B1, B2, G1, and G2)[3].

[1]Nutrition and Food Security Research Center, Isfahan University of Medical Sciences, Isfahan, Iran. [2]Department of Food Science and Technology, School of Nutrition and Food Science, Isfahan University of Medical Sciences, Isfahan, Iran. [3]Department of Environmental Health, Food Safety Division, School of Public Health, Tehran University of Medical Sciences, Tehran, Iran. [4]Department of Chemistry, Isfahan University of Technology, Isfahan 84154-83111, Iran. [5]Department of Food Science and Technology, National Nutrition and Food Technology Research Institute, Faculty of Nutrition Sciences and Food Technology, Shahid Beheshti University of Medical Sciences, Tehran, Iran. [6]Food and Drug Laboratory Research Center (FDLRC), IRAN FDA, Tehran, Iran. [7]Pharmaceutical Quality Assurance Research Center, The Institute of Pharmaceutical Sciences (TIPS), Tehran University of Medical Sciences, Tehran, Iran. ✉email: mahsaalikord@yahoo.com; nshariati@tums.ac.ir

Conventional methods for detecting aflatoxin presence, such as gas chromatography (GC), thin-layer chromatography (TLC)[4], high-performance liquid chromatography (HPLC)[5], liquid chromatography tandem mass spectrometry (LC–MS/MS)[6], and immunoassays like enzyme-linked immunosorbent assay (ELISA)[7], are often limited by their need for specialized equipment and trained personnel, as well as their time-consuming, large amounts of sample necessary for the extraction procedure (at least 100 g per analysis) and also high false-positive results are typical for the ELISA-based test-systems[7,8]. While LC-MS/MS offers excellent sensitivity and specificity for aflatoxin detection[9], like other conventional methods, it requires expensive instrumentation, complex sample preparation, and specialized expertise for operation and data interpretation.

These limitations make it challenging to improve extensive monitoring and investigation programs. One hopeful approach is biosensors and nano-biosensors. These techniques combine biological and nonmaterial components, such as antibodies, aptamers, enzymes, and nanoparticles, with chromophores that specifically and selectively bind to AFs[1,10]. When AFs bind to the recognition element, a signal is generated, which can be measured by the transducer and provides a quantitative measurement of aflatoxin contamination. Optical, electrochemical, and nanomaterial biosensors are different types of sensors for AFs detection that have been developed in recent years[11]. These biosensors have several advantages, such as rapid detection, high sensitivity, and specificity, as well as the potential for miniaturization and portability, making them suitable for on-site testing and real-time monitoring of aflatoxin contamination in food production and processing facilities[12].

Various color-recording devices including scanners[13], digital cameras[14], and smartphones[15,16] have emerged as valuable tools for rapid quantitative chemical analysis[17], chemical and biosensing[15], food diagnostics[18] and water analysis[19]. Among these, smartphone-based digital image colorimetry (DIC) has gained particular attention for its potential in on-site testing of food contaminants[20]. DIC utilizes smartphone camera capabilities and image processing algorithms to convert color intensity into numerical values for analyte quantification. The integration of DIC with dispersive liquid–liquid microextraction (DLLME) has shown promising results in recent studies[20,21]. DLLME offers significant advantages including rapid processing, minimal sample requirements, reduced solvent consumption, and high preconcentration factors while maintaining operational simplicity and cost-effectiveness[22]. The selectivity of DLLME is achieved through multiple mechanisms such as the partitioning behavior of analytes between the extraction solvent and aqueous phase based on their distribution coefficients, the optimization of extraction parameters including pH and ionic strength, and the effective removal of matrix interferents during phase separation[23,24]. These selective extraction capabilities, combined with significant preconcentration factors, enhance the analytical performance of the subsequent colorimetric detection. The combination of DIC's portable analytical capabilities with DLLME's efficient sample preparation, when coupled with nano-biosensors' specific recognition properties, creates a powerful analytical platform. This integrated approach enables the development of rapid, portable, and environmentally friendly methods for on-site detection of hazardous substances[21,25].

In this study, we present a new analytical approach combining three innovative elements: (1) biologically synthesized ZnO nanoparticles functionalized with curcumin, a natural dye from turmeric (*Curcuma longa*) (2). DLLME for efficient sample preparation and preconcentration, and (3) smartphone-based DIC for rapid and portable detection. This integrated system offers several advantages over conventional methods, including enhanced sensitivity and selectivity through the unique properties of bio-ZnO-NPs/curcumin composite, efficient sample preparation via DLLME, and cost-effective, on-site detection capabilities through smartphone-based colorimetry. The method was specifically developed and validated for AFB1 detection in baby food samples, addressing the critical need for rapid and reliable monitoring in this sensitive food category.

Results

Characterization of ZnO-NPs-P synthesis

Dynamic light scattering (DLS) analysis demonstrated that the biosynthesized zinc oxide nanoparticles from fermented table olive extract exhibited a bimodal size distribution, with populations in the 9–100 nm range and a hydrodynamic diameter of 150.6 nm. The nanoparticles' colloidal stability was confirmed by a −10.96 mV zeta potential and negative surface charge. A polydispersity index of 0.240 indicated relatively uniform size distribution (Fig. 1).

UV–Visible spectroscopy revealed a characteristic absorption peak at 370 nm (Fig. 2). The band gap energy, calculated using Tauc's relation[26], was determined to be 2.86 eV.

X-ray diffraction patterns revealed a hexagonal wurtzite crystal structure with an average crystallite size of 22.05 nm (Fig. 2).

FTIR spectroscopic analysis confirmed the presence of phytochemical compounds from the fermented table olive extract, which functioned as capping and stabilizing agents (Fig. 3).

FE-SEM and TEM imaging demonstrated spherical morphology with uniform size distribution, while EDX analysis confirmed the presence of zinc and oxygen elements in the biosynthesized samples (Fig. 4).

Optimization of the solvent used in nanoparticle and curcumin solution I and II

The optimization of solvents used in nanoparticle and curcumin solutions played a critical role in the detection system. According to the studies, a non-polar extraction solvent was necessary for AFB1 extraction in the DLLME system[27]. Previous colorimetric detection studies with ZnO-NPs used deionized water as a solvent[28], but this solvent was not suitable for our research. The octanol solvent produced gel with nanoparticles, and with chloroform, also the sedimentation of ZnO-NPs was observed in the solvent. Among the solvents investigated, hexyl acetate was the most suitable solvent as a proper solution for the ZnO-NPs (Fig. 5). For curcumin solvents (I) and (II), ethanol and methanol were selected, respectively. A mixture of 3 mL of 0.1 M NaOH, 1 mL of 0.1 M boric acid, and 2 mL of curcumin (mg/mL) in ethanol was prepared. 1:7 ratio of curcumin solvent (I) to methanol was selected as curcumin solvent (II)[28–30] (Fig. 6).

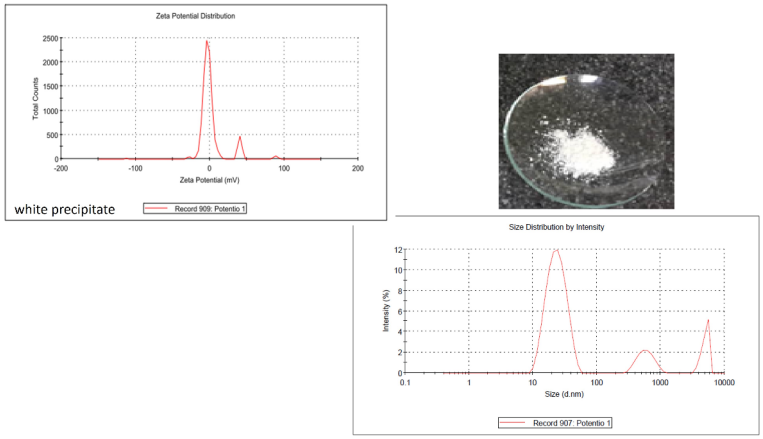

Fig. 1. Size measurement and Zeta Potential of the ZnO-NPs.

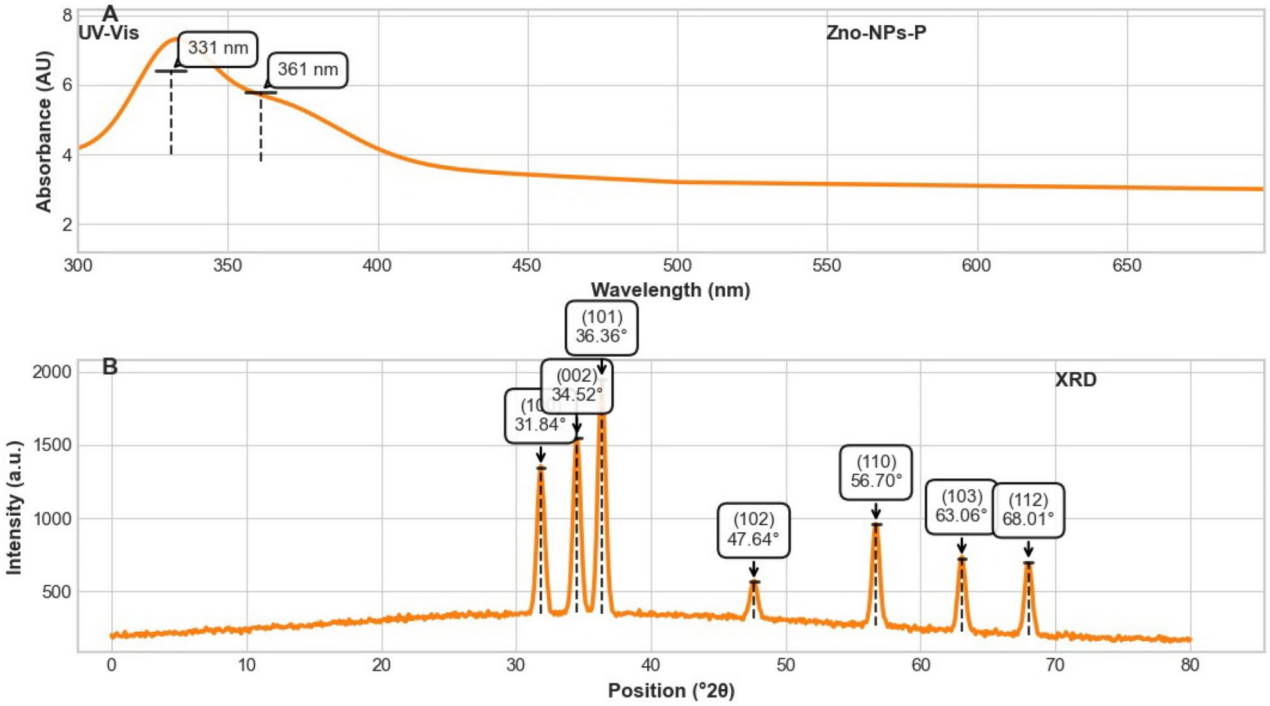

Fig. 2. The UV–visible spectrum and XRD of the ZnO-NPs.

Optimization of ZnO-NPs/curcumin nano-biosensor

The optimal efficiency of the condition of the ZnO-NPs/curcumin nano-biosensor complex was attained through the systematic evaluation of various parameters, including the ratio of curcumin to the nanoparticle, nanoparticle concentration, curcumin concentration, sensor pH, sensor reaction time, and sensor sensitivity with different concentrations of AFB1. Therefore, the results showed that the 2:1 ratio of curcumin (1 mg/mL) to ZnO-NPs (0.5 mg/mL) complex produced the highest and most separated absorbance at 368 nm in different concentrations of standards (Fig. 7s–9s). Furthermore, the optimal pH and reaction time showed 9.44 and 2–3 min, respectively (Fig. 9s). The optimized conditions enabled the sensor to exhibit high sensitivity towards AFB1, with a systematic increase in absorbance observed with increasing concentrations of AFB1 (Fig. 10s and 11s).

Optimization of SDIC conditions

Selection of the RGB channel and data processing method

Preliminary statistical analysis revealed a linear relationship between the concentration of AFB1 and color variables derived from the green channel (G), such as log (G), G/R, or G/Itot ratios. Although other color spaces (e.g., Lab, CMYK) were also explored, the single G channel showed the best linear response with a satisfactory coefficient of determination. The intensity of the signals (I) was measured based on the RGB channels, where

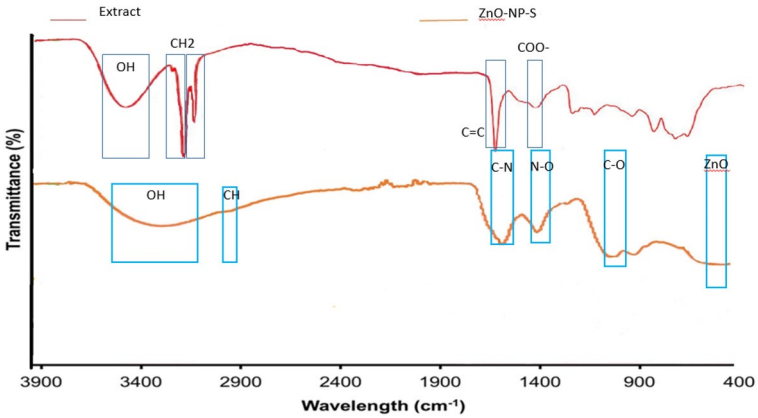

Fig. 3. FTIR of the ZnO-NPs.

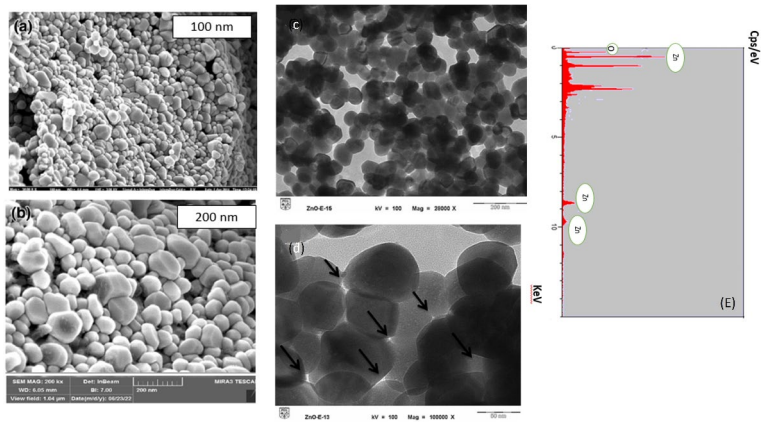

Fig. 4. FE-SEM (**a**, **b**), TEM (**c**, **d**) and EDAX (E).

Itot (sum of R + G + B intensities) equals 255 in the 8-bit color system[31], with the G channel showing the highest intensity (G/Itot = 0.45 ± 0.02) for AFB1 detection. This approach follows established methods in digital image colorimetry (Figure 12s).

Number and position of LEDs
According to the absolute darkness in the designed box, the number of light-emitting diodes has been tested, and according to the results obtained when sufficient light was provided to image the sample when the best angle is 45°. In other angles, it will not be possible to take a direct image with the necessary resolution and quality due to the inappropriate distribution of light relative to the sample location. Three images of the sample were obtained for each lighting condition (Figure 13s).

Distance between the camera and the cuvette
In addition to the lighting conditions, the distance between the smartphone camera and the sample solution[32], it was also studied by placing the camera at a distance of 6, 9, and 12 cm from the sample. When the camera was placed near the sample (5 cm distance), a blurred image was obtained, and the quality of the image improved as the distance increased (Figure 13s).

Optimization of DLLME- SDIC conditions

The SDIC-DLLME conditions were optimized using a standard solution of AFB1, which resulted in a response (R) or intensity signal (I). It enabled a precise observation of the impact of each parameter on the response.

Type and volume of extraction solvent
In DLLME, maximum recovery of the analyte in the extraction solvent is desired to maximize the method's sensitivity (Figure 14s). As can be seen in Figure 14s, chloroform formed the most stable cloudy solution and response among these three solvents[27,33], and finally, this solvent was selected as the extracting solution.

Also, to optimize the volume of extracting solvent, different volumes of chloroform were studied in the range of 150–350 µL. The highest extraction efficiency in the volume of chloroform solution 250 µL was obtained. After

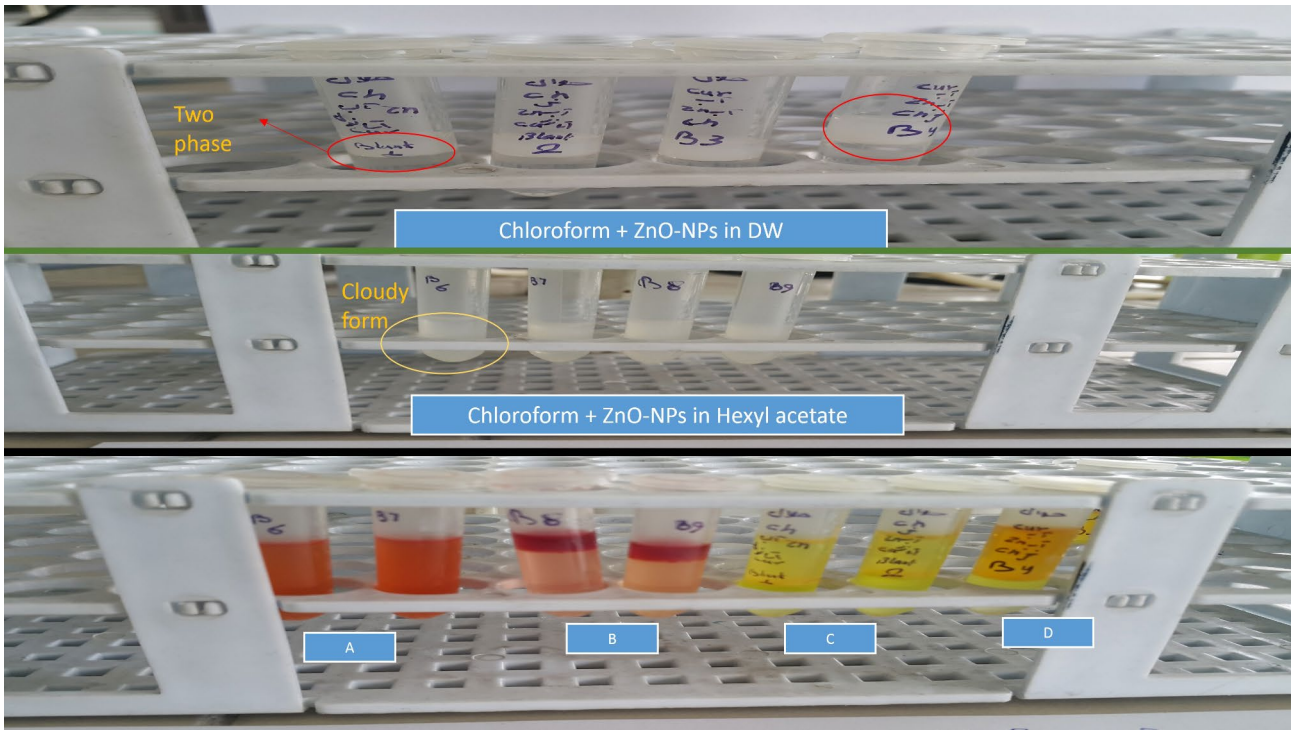

Fig. 5. Optimization ZnO-NPs solution.

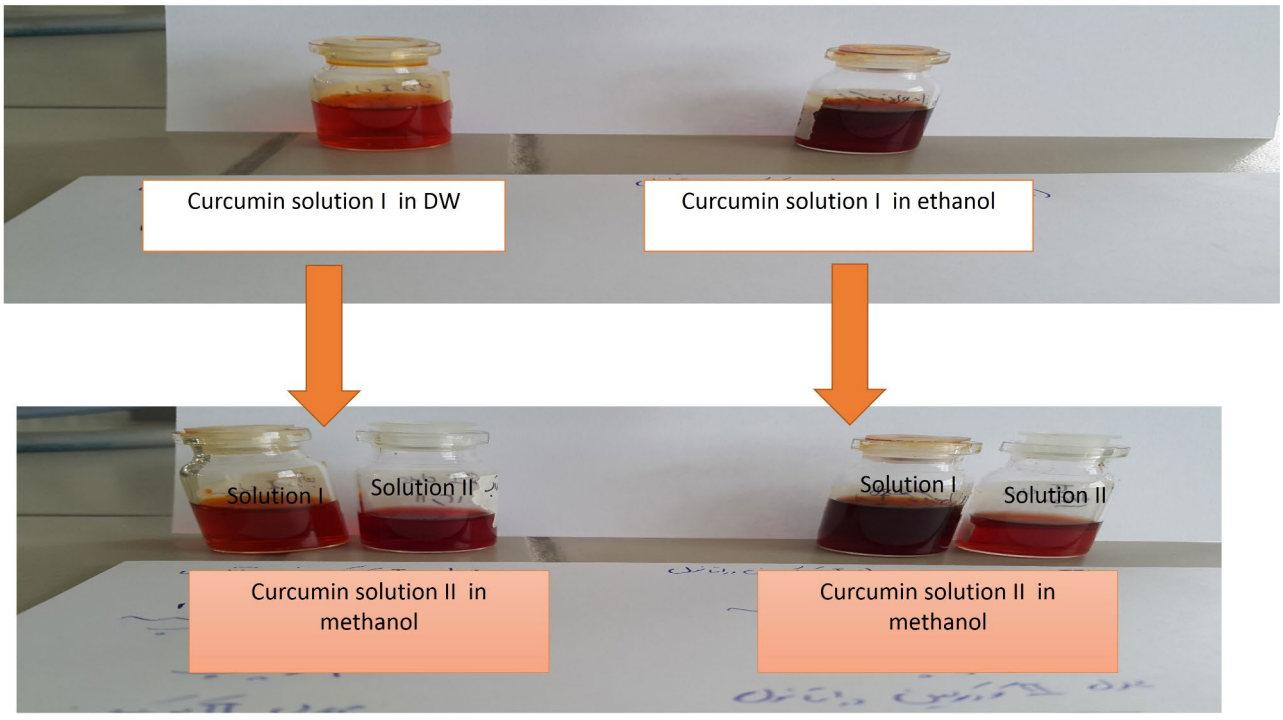

Fig. 6. Optimization curcumin solution.

Aflatoxin	Regression	R^2	LOD (µg/kg)	LOQ (µg/kg)	Intra-day (RSD%, n = 3)	Inter-day (RSD%, n = 3)
B1	y = 42.065x + 3.465	0.9906	0.09	0.27	5.52 ± 0.45	6.45 ± 0.42

Table 1. Results of sensitivity and reproducibility of the method.

Sample	AFB_1 spiked (µg/kg)	AFB_1 found (µg/kg)	References (µg/kg)	Recovery percentage%
Baby food	–	ND	ND	–
	0.5	0.45	0.51	89.89
	1	0.98	1.04	94.23

Table 2. Recovery percentage.

that the analysis signal slowly decreased. A representative volume of each solvent was collected after extraction and analyzed with SDIC (Figure 14s).

Type and volume of disperser solvent
The role of the disperser solvent in DLLME-SDIC is to increase the contact area between the immiscible extraction solvent and the aqueous sample solution, which increases the extraction efficiency of the analyte. 80% ACN and 80% MeOH in the range of 0.5–1.5 mL[27,33], which were used to extract AFB1, as the dispersed phase 1 mL of 80% ACN showing the best efficiency (Figure 14s).

Effect of pH
Based on the principles of the Henderson-Hasselbalch equation, at a pH that is at least two units below the pKa value of AFB1, which is reported to be around 7.2–9.29, the majority (approximately 99%) of AFB1 molecules will exist in their neutral and un-ionized form[33]. pH 9 showed the best analytical signal (Figure 15s).

Volume of sample and % W/V NaCl
As shown in Figure 15s, the analytical signal varied across different sample volumes (5-30 mL), with 20 mL providing the optimal analytical response.

The effect of NaCl concentration on the analytical signal is also depicted in the Figure 15s. The results indicate that a concentration of 2% w/v NaCl yields the highest analytical signal. Lower concentrations (0% and 1% w/v) show a noticeable decrease in analytical performance, while concentrations above 2% do not lead to any significant improvements.

Extraction time and centrifugation time
The extraction time in the DLLME procedure refers to the interval time between injections of the disperser and the extraction into the aqueous sample and starting to centrifuge. The effect of centrifugation time on extraction recovery was examined throughout the range of 1–5 min. Figure 15s indicated that the sample mixture was centrifuged for 3 min at 5000 rpm to reach a clear phase separation.

Analytical performance
In order to check the linearity of the response of the device, concentration ranges of the standard AFB1 (0, 0.05, 0.1, 0.15, 0.2, 0.4, 0.6, 0.8, 1 µg/L) in three repeats were assessed with the sensor and smartphone (Figure 16s) (Table 1).

Application to actual samples
HPLC was used for comparison and accuracy check. Comparable LODs, LOQs, R^2, and %RSD, were obtained, indicating similar analytical performance of both techniques (Figure 17s) (Table 2).

Interference study
The interference study results are summarized in Table 3. The interference study demonstrated that the developed SDIC-DLLME method coupled with the ZnO-NPs/curcumin nano-biosensor exhibits good selectivity for AFB1 in the presence of potential interferents commonly found in baby food matrices.

Discussion
Characterization of ZnO-NPs-P synthesis
The DLS findings demonstrate successful synthesis of zinc oxide nanoparticles with appropriate size and uniform distribution. The negative zeta potential indicates acceptable stability of the nanoparticles in solution, which is crucial for subsequent applications. The obtained particle sizes align with similar studies in this field[34]. The observation of an absorption peak at 370 nm and band gap energy of 2.86 eV confirms the quantum confinement effect, where decreased particle size results in increased band gap energy. In semiconductors, the band gap energy determines the minimum energy required for electron excitation from the valence to conduction band. The band gap energy of ZnO-NPs synthesized with extract increases by means of decreasing particle size, which is due to size limitation. This leads to a blue shift in the absorption spectrum of nanoparticles and an increase in

Interfere	Concentration relative to AFB1	Recovery rate (%)
AFB2	10x	98.7 ± 2.1
	50x	97.9 ± 2.5
	100x	96.5 ± 3.2
AFG1	10x	101.2 ± 1.8
	50x	104.5 ± 2.7
	100x	108.7 ± 3.5
AFG2	10x	99.5 ± 1.6
	50x	98.8 ± 2.3
	100x	97.2 ± 2.9
Casein	10x	98.1 ± 1.9
	50x	95.8 ± 2.6
	100x	93.8 ± 3.1
Whey protein	10x	99.3 ± 1.7
	50x	98.7 ± 2.2
	100x	97.5 ± 2.8
Vitamin A	100x	101.5 ± 2.3
Vitamin C	100x	99.8 ± 1.9
Iron (Fe)	10x	98.9 ± 1.5
	100x	102.8 ± 2.7
Zinc (Zn)	100x	100.7 ± 2.1
Calcium	10x	101.5 ± 1.2
	100x	102.3 ± 1.9

Table 3. Recovery rates of AFB1 in the presence of potential interferes. X: Concentration relative to AFB1.

the wavelength of light absorbed by nanoparticles. In other words, as the particle size decreases, less energy is required to absorb light. In semiconductors, the energy of the band gap determines the minimum energy needed to excite an electron from the valence band to the conduction band and therefore the maximum energy of the absorbable photon[35]. When the band energy decreases, nanoparticles can absorb photons with lower energy, which leads to an increase in overall light absorption in the material. FTIR analysis showed the presence of phytochemicals in the fermented table olive extract, which were involved in capping and stabilizing the ZnO-NPs[36]. The observed crystalline structure and uniform spherical morphology indicate well-controlled synthesis processes. These structural and morphological characteristics could facilitate potential applications of these nanoparticles across various fields[26,34,35]. The nanoparticles present in the cellular biomass are homogeneously accumulated and lead to the formation of a hierarchical sheet-like appearance. Many biomass nanoparticles appear to be quasi-spherical. The spaces or voids between the particles are identified, which are considered to be created by the aggregation between the biomass nanoparticles[37].

Construction of the colorimetric nano-biosensor detection system

In this study, ZnO-NPs were synthesized and mixed with curcumin solution to form a composite. The unique ZnO-NPs optical properties, such as their high surface area and high refractive index, make them a perfect material for sensing applications. Indeed, the high surface area of the ZnO-NPs allows for the efficient binding of target molecules, resulting in a color change that can be easily detected (Fig. 2A). The sensing mechanism involved in this complex is the electrostatic binding of phenolate anions of AFB1 with the oxidized curcumin in the presence of ZnO-NPs, resulting in a color change from red to yellow. The ZnO- NPs play a crucial role in enhancing the sensitivity of the sensor by providing a large surface area for the binding of AFB1 and curcumin. The curcumin, acts as a chromogenic agent, allowing for the visual detection of AFB1. The interaction between curcumin and ZnO-NPs in alkaline conditions led to the formation of a stable complex, which is vital for the sensing mechanism. The enol form of curcumin, presented in alkaline conditions by adding methanol to curcumin, experienced an oxidation reaction with ZnO-NPs, resulting in an oxidized product. Additionally, the AFB1 structure experienced alkali hydrolysis, leading to forming a phenolate anion, which is a kind of substituted coumaric acid. The electrostatic interaction between the phenolate anion and the oxidized product of curcumin in the presence of ZnO NPs finally led to the formation of a stable complex[28,35]. The other study found that the band gap energy of ZnO-NPs decreases with decreasing particle size, resulting in a blue shift in the absorption spectrum and increased light absorption at longer wavelengths[28]. Biosynthesized ZnO-NPs can be functionalized to target specific analytes to bind with specific ligands, making them a versatile platform for sensing applications[29]. Furthermore, the biocompatibility and non-toxicity of the biosynthesized ZnO-NPs make them an attractive material for biomedical and detection applications. The green synthesized ZnO-NPs exhibited remarkable characteristics such as rendering them suitable for applications in colorimetric sensors with curcumin acts as a chromogenic agent for detection[38–40]. The simplicity and economic feasibility of the analytical detection systems, including UV–VIS spectrophotometry and hand colorimetry, make them applicable in various food safety and quality analysis applications[30].

Optimization of the solvent used in nanoparticle and curcumin solution I and II

Curcumin is a lipophilic compound with limited water solubility. The curcumin solution and the extraction solvent, hexyl acetate, form a single phase and enable proper extraction and identification phase in the DLLME system[29]. Ethanol and methanol are commonly used solvents for curcumin due to their ability to dissolve and solubilize this compound effectively[41]. Also, the 1:7 ratio of curcumin solvent (I) to curcumin solvent (II), is supported by the findings from the referenced studies[29], which demonstrate the changing color effectiveness and their ratio in enhancing the solubility and extraction of curcumin.

Optimization of Zno-NPs/curcumin nano-biosensor

This optimization of the nano-biosensor has essential effects the detection of AFB1[29]. Indeed, the use of simple and commercial detection techniques, such as UV-Vis spectrophotometry and hand colorimetry, makes it reasonable, its ease of use and portability for common applications. In addition, the results showed the ability to detect AFB1 at concentrations lower than 0.0001 µg/L, which emphasizes the potential of this sensor for early warning systems in food safety monitoring[30].

Optimization of SDIC conditions

To process the data, a formula was used to calculate the response (R) or the intensity of the signals, which takes into account the intensity of the signals obtained from the G channel for both the blank and sample solutions. The linear correlation coefficient in the G parameter was higher than that of the R parameter (Figure 12s). The G parameter also showed a larger magnitude and difference in the number of observations, leading to a more reliable conclusion at lower concentrations. Therefore, the G parameter was selected as the default for further studies. All results were evaluated using absolute values. It is possible because the green color is complements the AFB1 nano-biosensor complex, resulting in a linear response.

It is important to note that selecting an appropriate instrumental response is crucial when applying smartphone colorimetric to a particular color hue series. While previous studies have shown that converting device-dependent RGB signals to device-independent, uniform color space signals can enhance calibration linearity and sensitivity, no significant improvement was observed in this study when using other color spaces instead of RGB[20]. It may be due to the uniform and stable measuring environment provided by the homemade box, which reduced the impact of differences in smartphone hardware and quantitative models.

In various studies, several methods have been used to process the data from the selected channel. For example, using Beer's law or the formula $R = 255 - I$[42] or $R = IG_b - IG$[21,43]. The first formula assumes that the blank is white space, which is not true in most practical situations. The signal obtained with the blank was always less than 255, which even with a sample containing the analyte at a concentration below the limit of detection (LOD) of the method, resulted in a high intercept in the calibration graph. In the second formula, also used in this study, IG_b and IG are the intensity of the signals obtained from the green channel for the blank solution and the sample solution, respectively[20,21].

The accuracy of the obtained peak areas was calculated. In addition, the effect of light intensity was evaluated by lighting different numbers of LEDs (8, 6, and 4)[21,32]. In addition, when enough light provided to take an image of the sample, six light-emitting diodes were placed in two groups on 45° of the container on the sides of the sample container. The light layout can efficiently eliminate any effect from reflected light occurring and avoid the consequent lensing effect resulting from bottom light after optimization (Fig. 13s).

However, a focal length of 9 cm was considered appropriate because a longer length required a larger size of the photographic box and, in addition, camera magnification on the sample solution was needed, resulting in an unclear image. The best result regarding image accuracy and repeatability of the analysis signal was obtained when the smartphone was placed at a distance of 9 cm from the sample container (Fig. 13s).

Optimization of DLLME–SDIC conditions

As can be seen in Fig. 14s, chloroform formed the most stable cloudy solution and response among these three solvents[27,33], and finally, this solvent was selected as the extracting solution.

Also, to optimize the volume of extracting solvent, different volumes of chloroform were studied in the range of 150–350 µL. The highest extraction efficiency in the volume of chloroform solution 250 µL was obtained. After that the analysis signal slowly decreased. A representative volume of each solvent was collected after extraction and analyzed with SDIC (Fig. 14s).

The highest response was obtained with ACN (80%)[27,33]. To investigate the effect of the volume of the dispersant solution, different volumes of ACN were studied in the range of 0.5–1.5 mL, which finally showed the best extraction efficiency in 1 mL. Further increase resulted in decreased in the response (Figure 14s), which was thought to be due to increased solubility of AFB1 in the aqueous solution in the presence of higher concentrations of ACN. Therefore, a volume of 1 mL was selected for further experiments. The disperser solvent in DLLME–SDIC plays a critical role in the formation of fine droplets of extraction solvent within the aqueous sample solution, thereby facilitating efficient mass transfer through increased surface area contact[44]. Based on preliminary experiments and previous studies, 80% ACN and 80% MeOH were selected as disperser solvents. The selection of these binary mixtures over pure organic solvents was supported by several analytical considerations: the binary solvent systems provided optimal polarity for AFB1 extraction as demonstrated by Sajid[45], enhanced cloud point formation and phase separation efficiency as reported by Wang et al.[46], and explained compatibility with the aqueous sample matrix according to Rykowska et al.[47] The extraction performance of different disperser solvent compositions was evaluated.

The maximum extraction efficiency of DLLME was obtained when the pH of the aqueous phase was kept at pH 9. The chromogenic reaction of AFB1 and nano-biosensor is usually carried out under alkaline conditions; thus, pH has primary influence on the extraction efficiency[28].

As shown in Figure 15s, the analytical signal showed volume-dependent behavior across the studied range (5–30 mL). The highest analytical signal is observed at a sample volume of 20 mL, indicating that this volume is optimal for the detection process. Similar findings have been reported in previous studies where optimal sample volumes were identified to balance sensitivity and analytical performance[48]. Higher sample volumes led to decreased extraction efficiency, likely due to dilution effects and reduced phase transfer kinetics[49,50]. This optimization aligns with previous DLLME studies for similar analytes[51].

The results suggest that NaCl plays a crucial role in optimizing the extraction process and enhancing the solubility of aflatoxin B1 in the sample matrix. Other studies have suggested that ionic strength, influenced by NaCl concentration, can significantly affect the extraction efficiency and specificity of analytes in complex matrices[52].

The response increased with the increasing extraction time from 1 up to 3 min but remained almost decrees afterward, indicating the variations of longer vortex agitating time were not significant. Therefore, an extraction time of 3 min at 5000 rpm was considered optimum in subsequent experiments[27,33].

Analytical performance

The calibration curve demonstrated strong linearity with a correlation coefficient (R2) of 0.9906 across the tested concentrations. The analytical sensitivity was evaluated through limit of detection (LOD) and limit of quantification (LOQ) calculations, derived from the response standard deviation and calibration curve slope. The method achieved LOD and LOQ values of 0.09 and 0.27 µg/kg respectively for AFB1 (Table 1). These sensitivity parameters compare favorably with recent studies in the field. Peng et al. (2019) achieved LODs of 0.017 µg/mL using DLLME–DIC for calcium analysis in water and food samples[20], while Hamed et al. (2019) reported LODs of 0.5 µg/kg using DLLME–HPLC detection in plant-based milk and dairy products without nanoparticle adsorption[53]. Furthermore, Zhao et al. (2016) demonstrated LODs ranging from 0.087 to 0.632 ng/mL for various aflatoxins using ionic-liquid-based DLLME combined with magnetic SPE[54]. The enhanced sensitivity in our method can be attributed to several factors such as the efficient preconcentration achieved through optimized DLLME conditions[51]. Recent advancements have seen the integration of nanomaterials, such as gold nanoparticles and carbon dots, into smartphone-based detection systems. For instance, Chaisiwamongkhol et al. (2020) demonstrated the effectiveness of gold nanoparticles for colorimetric detection of substances like sibutramine in food supplements, showcasing the potential of smartphone-based applications in food safety monitoring[55]. Similarly, Solanki et al. (2024) explored the use of carbon dot nanomaterials for food safety analysis using smartphone techniques, further emphasizing the versatility and efficiency of these innovative approaches in analytical chemistry[56]. The signal amplification provided by the ZnO–curcumin nanobiosensor system, and the controlled imaging conditions that improved the signal-to-noise ratio[57].The recovery percentage for AFB1 was calculated between 89.8-94.2% (Table 1). Additionally, the %RSD values obtained for intra-day and inter-day measurements (n = 3) were always less than 6% and 7%, respectively, which proves that the proposed method is precise.

Application to actual samples

Baby food samples were selected for AFB1 detection due to their significance in food safety monitoring, particularly for vulnerable infant populations, as aflatoxins pose serious health risks to developing children[58]. Our developed ZnO-NPs-curcumin–DLLME–SDIC method demonstrated excellent sensitivity with LOD of 0.0183 ± 0.00577 ng/mL in spiked samples (0, 0.5 and 1 ng/mL). Additionally, Cheng et al. (2022) demonstrated comparable sensitivity using a colorimetric/fluorescence dual-mode immunoassay based on streptavidin-induced gold nanoparticle aggregation for AFB1 detection, achieving LODs of 6.95 ng/mL and 0.07 ng/mL for colorimetric and fluorescence detection respectively, though our approach offers significant advantages in terms of cost-effectiveness and operational simplicity[59]. The statistical comparison between the proposed method and reference techniques showed good agreement ($P > 0.05$), validating its reliability for routine analysis.

Matrix effects, which commonly influence mycotoxin detection in complex food samples, were carefully evaluated. The slope of the matrix-matched calibration curve (0.0412) was 7.8% lower than that of the standard calibration curve in pure solvent (0.0447), indicating a moderate matrix effect. This matrix effect was consistent across different types of baby food samples with relative standard deviations less than 5%. To ensure accurate quantification, matrix-matched calibration was employed following established protocols for mycotoxin analysis in complex food matrices[60,61].

Interference study

Most tested substances did not significantly interfere with AFB1 detection, showing recovery rates within the range of 95-105%. However, AFG1 at 100 times the concentration of AFB1 caused a positive interference (+8.7% signal change), likely due to structural similarities. Among the proteins, casein at high concentrations (100x) resulted in a slight negative interference (− 6.2%). Vitamins and minerals generally showed minimal interference, with recovery rates ranging from 97.5 to 102.8%.

The high recovery rates (95–105%) for most tested substances indicate minimal matrix effects, which is crucial for accurate AFB1 quantification in complex food samples[62]. The slight positive interference observed with AFG1 at high concentrations is consistent with previous studies reporting cross-reactivity between structurally similar aflatoxins[63]. The minor negative interference caused by casein at high concentrations may be attributed to protein-AFB1 interactions, as reported by Wu et al.[62]. The optimized pH (9.4) likely contributed to the method's selectivity by enhancing AFB1 extraction while minimizing interferences. Overall, the developed method demonstrates robust performance in the presence of potential interferents, making it suitable for AFB1 detection in baby food samples. However, further validation with a wider range of food matrices is recommended to ensure broad applicability.

Method	Type	LOD (ng/mL)	Analyte	References
Enzyme-linked immunosorbent assay	Peanut	0.05	AFB1-G1	[67]
Chemiluminescence-based immunoassay	Rice	0.0015	AFB1	[68]
Lateral flow immunoassay	Feed	5	AFB1	[69]
Fuorescence immunoassays	Peanut	0.008	AFB1	[70]
Immunochip	Water	0.01	AFB1-M1	[71]
Membrane-based assays	Corn	20	AFB1	[72]
Immunosensor (Cur–znobt)	Corn-Peanut	0.02 4.37- 2.74	AFB1	[29]
ZnO-NPs-cur	Rice	11	AFB1	[28]
starch–iodine paper-based analytical devices	corn, peanuts, pasta, Chinese Baijiu, soy sauce, and traditional Chinese food eight-treasure porridge	9.45	AFB1	[73]
Cur–TiO_2 NPs	peanut and corn	1.4	AFB1	[30]
Magnetic Bead-Based Immunoassays- Gold Nanoparticles	Maize	0.007	AFB1	[74]
Cur–ZnO-NPs + DLLME	Baby food	0.09	AFB1	This study

Table 4. Comparison of the studied method with other methods.

Comparison with other methods

Recent literature demonstrates significant advancements in combining digital image colorimetry with various liquid-phase microextraction techniques for analytical applications. For instance, Jain et al. (2023) developed a non-instrumental SA-DLLME-TLC-SDIC method for favipiravir detection, achieving LODs of 1.2–1.5 µg/spot in biological samples[64]. In environmental analysis, Zhao et al. (2023) introduced an eco-friendly approach using deep eutectic solvent-based DLLME coupled with smartphone colorimetry for carbofuran detection, reaching LODs of 0.024–0.032 mg/L in water samples[65]. Jing et al. further expanded this field by implementing bio-derived solvent-based DLLME with smartphone colorimetry for carbofuran detection in cereals, achieving impressive LODs of 0.005 mg/kg[66]. These studies collectively highlight the growing trend of integrating smartphone-based colorimetry with microextraction techniques, offering sensitive, cost-effective, and environmentally friendly analytical solutions.

The efficiency of the proposed method was also compared with other methods reported in the literature for the determination of AFB1, considering aspects such as analysis time, sensitivity, linearity, and repeatability (Table 4). In this study, the proposed method for measuring AFB1 with a light control box, battery, and sensor has been compared with other methods. The advantages of the proposed method include low solvent and sample consumption, simplicity, high speed, low cost, and easy accessibility. Also, the ability of this method to analyze in outside the laboratory compared to other common methods such as visible-ultraviolet spectrometer and liquid chromatography method are higher. The results showed that the proposed method can be considered as one of the methods in terms of high accuracy and speed, low cost and easy access to be used for AFB1 in food samples. Comparison of this method with other common methods, merit figures of the proposed method such as detection limit, linear region, and accuracy of the method, along with details such as analysis method, extraction method, and on-site analysis capability. The main advantages of this method over the others included rapidness, simplicity, and cost-effectiveness.

Materials and methods

Chemicals and reagents

De Man, Rogosa and Sharpe culture medium (MRS) broth, peptone (≥ 99%), absolute ethanol (≥ 99.8%), ethanol (70%), curcumin (≥ 94%), boric acid (≥ 99.5%), methanol (MeOH, ≥ 99.9%), chloroform (≥ 99.8%), hexyl acetate (≥ 99%), octanol (≥ 99%), aflatoxin B1 standard (AFB1, ≥ 98%), tetrachlorobenzene (≥ 98%), tetrachloroethylene (≥ 99%), hydrochloric acid (HCl, 37%), isopropanol (≥ 99.5%), sodium hydroxide (NaOH, ≥ 98%), sodium chloride (NaCl, ≥ 99.5%), n-hexane (≥ 95%), zinc sulfate heptahydrate (ZnSO4.7H2O, ≥ 99%), and acetonitrile (ACN, ≥ 99.9%) were obtained from Merck (Darmstadt, Germany). All chemicals and reagents used were of analytical grade or higher purity. Deionized water was used throughout the experiments, produced by a Millipore Milli-Q water purification system (Bedford, MA, USA).

Instrumentation

Sonication was completed with an ultrasonic bath (Isolab, Eschau, Germany), a pH meter (PHS-3C, Jinke, Shanghai, China) was used to measure pH. The vortex mixing was done with an MS 3 digital vortex (IKA, Staufen, Germany). A hotplate is used for heating during sample digestion. Centrifugation was performed with an EBA20 Portable Centrifuge C2002 (Hettich, Tuttlingen, Germany) to accelerate the process of phase separation. The samples and standards were weighed using an electronic balance (Mettler-Toledo, Greifensee, Switzerland). An incubator with a shaker (PIT053RS, Pole Ideal Pars Co, Tehran, Iran) was used, and the optical densities (OD) at 200-700 nm were measured.

Digital images of color sample solution used with Samsung S21 FE smartphone. The primary camera of this phone has an aperture of f/1.8 and a resolution of 50 megapixels. Also, the Dynamic AMOLED 2X display of this phone has dimensions of 6.4 inches and a resolution of 1080 × 2340 pixels. This phone has a large image sensor,

a powerful Exynos 2100 chipset with a speed of up to 2.91 GHz, 128/256 GB of internal memory, and 6/8 GB of RAM capacity.

Apparatus

The basis for reproducibility in imaging and the resulting results is an environment with uniform and constant light. A colorimetric wood box with the sizes of 20 × 20 × 20 cm was designed to capture reproducible digital images of standard and sample solutions. The box`s interior was painted black to minimize light scattering. A small hole was drilled on the side of the box for capturing images of sample solutions placed into a 10.0 mm quartz UV/Vis microcuvette (Hellma, Kruibeke, Belgium), which was located inside the box in optimized distances (cm) from the detection camera. The holder frame was used in the front of the box to keep the smartphone stable and fine-tuned. To avoid reflection from the surface of the colored sample to the glass test tube, the flashlight of the mobile phone camera was turned off while taking pictures. The most suitable lighting of the lamp was chosen, that is, the point where the analysis has the highest amount of the best color signal changes, and the distance was fixed at that place. Some battery-powered LED strip is placed at an optimized degree angle to the cell phone camera lens inside the box to serve as a constant light source to obtain uniform scattered light. Then, the sample was in a made holder and placed inside the photography box. Digital image and signal changes were prepared online.

Preparation of fermented olive fruit extract and zinc oxide nanoparticles

The procedure was carried out according to Alikord et al.[35] Fermented pitted olive fruits (10 g) were homogenized with 1 L of deionized water and heated at 80 °C for 10 min to obtain a greenish-white extract and cooled to room temperature. Then, the extract was filtered with Whatman paper (No. 42) and kept at the refrigerator temperature. $ZnSO_4{\cdot}7H_2O$ solutions (0.2) M were prepared under stirring conditions with a magnetic magnet at 25 ± 2 °C. Then, the solution was used in 2:1 ratio of $ZnSO_4{\cdot}7H_2O$ (0.2 M) and MRS broth containing olive extract. The mixture of MRS broth and $ZnSO_4{\cdot}7H_2O$ solution was adjusted to pH by 0.4 M NaOH to investigate the delay of the conversion process. The pH of MRS is 7.5, after adding the extract, it reached 4.7, and then the pH was adjusted to 12. The extract was gradually added to the $ZnSO_4{\cdot}7H_2O$ solution and MRS broth until the solution changed from reddish brown to white and suspended particles were observed. Finally, the solution was heated at 80 °C water bath for 5–10 min, and then incubated in a dark position at 37 °C for 24 h. The precipitate was sterilized and washed with deionized water and ethanol. All particles are collected at the bottom of the flask. Finally, the samples were centrifuged at 5000 rpm for 25 min and the cell biomass precipitate (P) was separated. Cell biomass was dried at 40 °C for 4–6 h. The sample without $ZnSO_4{\cdot}7H_2O$ was used as a negative control. The samples were kept in the dark in the refrigerator until the test and used in the next step.

Characterization of synthetic nanoparticles

The biosynthesized ZnO-NPs-Precipitate (ZnO-NPs-P) was thoroughly characterized using various analytical techniques. The hydrodynamic particle size distribution and polydispersity index (PDI) were determined using Dynamic Light Scattering (DLS) on a Malvern Instruments device (UK). Following 30 min of sonication and dilution, the zeta potential was measured. The formation and stability of ZnO-NPs were monitored using UV–Vis spectroscopy (Uviline 9400, Secomam, France) in the wavelength range of 200–700 nm, specifically employing surface plasmon excitation and UV–Vis spectroscopy (Uviline 9400, Secomam, France) using surface plasmon excitation in the wavelength range of 200–700 nm. Functional groups present in the nanoparticles were identified using Fourier Transform Infrared (FTIR) spectroscopy (Thermo Avatar, France) with potassium bromide as the pelletizing agent, under dehumidified conditions, in the spectral range of 400–4000 cm^{-1}. The crystal structure of the nanoparticles was analyzed using X-Ray Diffraction (XRD) on a 1930 PW generator with 1820 PW, utilizing fixed Cu Ka radiation. The morphology, size, and elemental composition of the ZnO-NPs were examined using Field Emission Scanning Electron Microscopy (FE-SEM) coupled with Energy Dispersive X-ray Analysis (EDAX) on a TESCAN MIRA3 instrument (USA). Furthermore, Transmission Electron Microscopy (TEM) analysis on a Philips EM 208S instrument was employed to investigate the internal structure of the nanoparticles and any amorphous matrix present.

Aflatoxin B1 standard solution

Stock solutions of aflatoxin B1 were prepared with a concentration of 10 µg/mL of methanol. The working concentrations of the prepared stock solution were stored in the freezer for further use.

Optimization of ZnO-nanoparticle solution

For the DLLME system, a solvent with the property of creating cloudy conditions in the extraction AFB1 was investigated. Indeed, to identify the best type of solvent for the nanoparticle part of the nano-biosensor, to create an appropriate system in DLLME, investigated four solvents, including hexyl acetate, octanol, chloroform, and deionized water.

Optimization of curcumin solution

The solution of curcumin (mg/mL) in water or ethanol was added to 3 mL NaOH (0.1 N) and 1 mL of 0.1 M boric acid for 2 min as a solution I. Then, solution (I) was mixed with methanol as solution (II) with a dilution rate of (1:5, 1:7, 1:10, 1:100, 1:200, 1:500, and 1:1000 mL/mL methanol) in optimization step and kept in a dark place. This part was also based on the entire nano-biosensor platform and extraction stage, the similar to the ZnO-nanoparticle solution.

Optimization of Zno-NPs/curcumin nano-biosensor

After determining the optimized solvents for nanoparticle and curcumin solutions to form a cloudy state in the DLLME stage, different variabes of ZnO-NPs/curcumin nano-biosensor were optimized. Ratios of 1:1, 1:2, and 2:1 of Zno-NPs solution and curcumin solution were prepared as well as 0.1 mL standard of AFB1 was added, and their absorbance was read visually by UV–Vis spectrometry at 200–700 nm. After choosing the appropriate ratio and the best wavelength (nm), nanoparticle concentration (0.2, 0.4, 0.6, 0.8, 1, and 1.2 mg/mL hexyl acetate), curcumin concentration (0.5,1, 1.5, 2, and 2.5 mg/mL ethanol), pH (8.8, 9, 9.2, 9.4, 9.6, 9.8 and 10) and reaction time (1, 2, 3, 4, and 5 min) of Zno-NPs/curcumin Nano-biosensor were also optimized. Finally, the sensitivity of the sensor in different concentrations of standard AFB1 (0.0001, 0.001, 0.01, 0.1, 1, 2, 3, 4, and 5 µg/L) was assessed.

Optimizing colorimetric box

The optimization of device parameters to obtain maximum response was assessed. The effect of the camera's distance from the sample container, the number and direction of LED exposure to the sample on the test results was investigated. The effect of the distance between the camera and the sample at distances of 4, 6, and 9 cm was studied to achieve a high-resolution image. The number of one to three of 4, 6, and 8 diodes in different directions of 0, 45, 90, and 180° angle relative to the sample container was investigated.

Sensing procedure and data processing

The reaction mixture of Zno-NPs/curcumin nano-biosensor prepared after optimization, was moved into the UV–Vis micro cuvette inside the colorimetric box for taking the photo of the solution with the smartphone camera as SDIC.

Color Grab is an easy operation and powerful of free color acquisition software that one touch shot can obtain RGB, Lab, CMYK and other, more than a dozen color space values with self-defined Region of Interest (ROI). The raw RGB values (R (red), G (green), and B (Blue)) were directly read out by the App on a smartphone for further quantitative analysis[20] without additional computational digital image transformation and process. Calibration curves for AFB1 quantification employing the current method were first built to evaluate the channels R, G, and B. According to the results, the highest level of sensitivity and linear range is obtained when the difference between the green or red channel of the control and the samples is used as the analysis signal. The horizontal ordinate represented the concentration of AFB1, in contrast the vertical ordinate represented the relative intensity of the G channel, normalized as follows: $I = (IG - IG\ blank)/255$. The blank intensity with normalization was linearly related to the AFB1 concentration. The linear relationship between AFB1 concentration and the relative intensity was constructed under optimal conditions.

Dispersive liquid–liquid microextraction procedure (DLLME)

In this research, the DLLME technique was used to extract and pre-concentrate AFB1 from baby food. DLLME involves the aqueous sample, an extracting solvent, and a dispersing solvent that can quickly form a cloudy solution. Then the cloudy solution is centrifuged, the supernatant is separated extracting solution containing the analyte was transferred to the microtube and then added to the Zno-NPs/curcumin Nano-biosensor. The extracting solvent containing AFB1 was transferred into the quartz micro cuvette for analysis with SDIC. The intensity of the analytical signal is checked in the homemade box and data processing.

Optimization of DLLME

To obtain the highest extraction efficiency in DLLME, various factors such as the type and volume of extracting solvent, the type and volume of dispersing solution, pH, and centrifuging time have been investigated in this research. Three different extraction solvents, including chloroform ($CHCl_3$), carbon tetrachloride (CCl_4), and tetrachloroethylene (C_2Cl_4) were studied. Also, to optimize the volume of extracting solvent, different volumes in the range of 150–350 µL were studied. The dispersion solution of 80% acetonitrile and 80% methanol were assessed. To investigate the effect of the volume of the dispersant solution, different volumes in the range of 0.5–1.5 mL were studied. Also, the impact of pH in the range of 3–9 and volume of sample as well as NaCl (% W/V) were studied to obtain the best extraction efficiency, and the centrifugation time in the range of 1–5 min at 5000 rpm was studied.

Analysis of actual sample and matrix effect

The baby food was completely homogeneous and uniform to extract. 25 g of the homogenous sample and 0.1 g NaCl were weighed, and 25 mL of 80% acetonitrile-water (80:20, v/v) was added to it and then mixed for 10 min in a magnetic shaker at medium speed. Then it was centrifuged (5000 rpm for 5 min), 10 mL of the upper layer with 6 mL of n-hexane was poured into a falcon tube for defatting and centrifuged again (5000 rpm for 5 min). The upper layer was separated and the remaining liquid was used for the DLLME step. The resulting solution was filtered using a Nylon micro-filter, it was used as a blank sample. Further spiked samples with different amounts of AFB1 concentrations (0, 0.5 and 1 µg/L) were rotated in a shaker for 3–4 h and extracted in the dark with a similar method to be used as analytical samples. Control and spiked samples were evaluated for method validation by nano-sensor and smartphone with high-performance liquid chromatography and FLD detector (HPLC–FLD).

The impact of sample matrix on the analytical performance was assessed using matrix-matched calibration curves. Baby food samples were spiked with AFB1 at concentrations ranging from 0 to 1 µg/L. The slopes of the matrix-matched calibration curves were compared to those obtained from standard solutions. Matrix effects were calculated as the percentage difference between the slopes.

Interference study

To evaluate the selectivity of the proposed method, an interference study was conducted using common components found in baby food matrices. The potential interferents tested included other aflatoxins (AFB2, AFG1, AFG2, ochratoxin A, zearalenone, and deoxynivalenol), proteins (casein, whey protein), vitamins (A and C), and minerals (Ca, Fe, and Zn). Standard solutions of AFB1 (1 µg/kg) were spiked with each potential interferent at concentrations 10, 50, and 100× higher than AFB1. The spiked samples were then analyzed using the optimized SDIC-DLLME method. The extraction was performed according to set method using chloroform (250 µL) as the extraction solvent and acetonitrile (1 mL) as the disperser solvent, with a 5 min extraction time. The pH was adjusted to 9.4 to optimize selectivity for AFB1. The ZnO-NPs/curcumin nano-biosensor was prepared using the optimized 2:1 ratio of curcumin (1 mg/mL) to ZnO-NPs (0.5 mg/mL). After extraction and color development, digital images were captured using the Samsung S21 FE smartphone under controlled lighting conditions in the colorimetric box. The images were analyzed using the optimized region of interest to quantify color changes. Recovery rates were calculated to assess the impact of potential interferents on AFB1 detection.

HPLC analysis

The HPLC system consisted of a fluorescence detector with an excitation wavelength of 365 nm and an emission wavelength of 418 nm. Chromatographic separation was performed using a gradient elution method with a mobile phase of water, acetonitrile, isopropanol, and 1% acetic acid. Mobile phase A was 91:1:1:7 (v/v) water/acetonitrile/isopropanol/1% acetic acid, and mobile phase B was 43:25:25:7 (v/v) water/acetonitrile/isopropanol/1% acetic acid. The gradient program started at 84% A and 16% B for 4.5 min, then linearly increased to 52.5% A and 47.5% B over 4.5 min, at a flow rate of 1.3 mL/min for 6 min and then 1 mL/min for the final 1 min. An injection volume of 20 µL was used. An internal standard of AFB1 at concentrations of 0.5 and 1 µg/L was also analyzed[19].

Method validation

For method validation, analysis of variance (ANOVA) was performed using SPSS software (version 17.0, https://www.ibm.com/products/spss-statistics), followed by Duncan's test to determine significant differences ($p < 0.05$). A calibration curve was plotted in the range of 0–1 µg/L using Excel (version 2013, https://www.microsoft.com/microsoft-365/excel). The coefficient of determination (R^2), regression equation, limit of detection (LOD), and limit of quantification (LOQ) were determined. Accuracy, expressed as percent recovery, was evaluated by spiking samples at three different concentration levels. Intra-day and inter-day precisions, expressed as percent relative standard deviation (%RSD), were studied at two concentration levels using three replicates. Accuracy was expressed as percent recovery and was evaluated by spiking a known amount of AFB1 in samples at different concentration levels.

Data availability

The datasets used and/or analysed during the current study available from the corresponding authors on reasonable request.

Received: 14 January 2025; Accepted: 4 March 2025
Published online: 19 March 2025

References

1. Zhu, H. et al. Spectral intelligent detection for aflatoxin B1 via contrastive learning based on Siamese network. *Food Chem.* **449**, 139171 (2024).
2. Ráduly, Z. et al. Toxicological and medical aspects of Aspergillus-derived mycotoxins entering the feed and food chain. *Front. Microbiol.* **10**, 2908 (2020).
3. Commission Regulation No 1881/2006 of 19 December 2006 setting maximum levels for certain contaminants in foodstuffs. Official Journal of the European Union, 364, 5. (2006).
4. Wacoo, A. P. et al. Methods for detection of aflatoxins in agricultural food crops. *J. Appl. Chem.* **1**, 706291 (2014).
5. Golge, O. et al. Determination of aflatoxins in walnut sujuk and Turkish delight by HPLC–FLD method. *Food Control.* **59**, 731–736 (2016).
6. Panda, D. et al. Recent advancements in LC-MS based analysis of biotoxins: Present and future challenges. *Mass Spectrom. Rev.* **41**(5), 766–803 (2022).
7. Baydar, T. et al. Aflatoxin B1, M1 and ochratoxin A levels in infant formulae and baby foods marketed in Ankara, Turkey. *J. Food Drug Anal.* **15**(1), 11 (2007).
8. Sun, J. et al. Sensitive detection of aflatoxin B1 in foods by aptasensing-based qPCR. *Food Chem.* **432**, 137240 (2024).
9. De Santis, B. et al. Development of a LC–MS/MS method for the multi-mycotoxin determination in composite cereal-based samples. *Toxins.* **9**(5), 169 (2017).
10. Wu, M. et al. An ultrasensitive electrochemical aptasensor based on zeolitic imidazolate framework-67 loading gold nanoparticles and horseradish peroxidase for detection of aflatoxin B1. *Food Chem.* **456**, 140039 (2024).
11. Sergeyeva, T. et al. Development of a smartphone-based biomimetic sensor for aflatoxin B1 detection using molecularly imprinted polymer membranes. *Talanta.* **201**, 204–210 (2019).
12. Dai, S. et al. A novel magnetic resonance tuning-magnetic relaxation switching sensor based on Gd-MOF/USPIO assembly for sensitive and convenient aflatoxin B1 detection. *Food Chem.* **443**, 138537 (2024).
13. Göröcs, Z. & Ozcan, A. Biomedical imaging and sensing using flatbed scanners. *Lab Chip.* **14**(17), 3248–3257 (2014).
14. Liñero, O. et al. The use of a standard digital camera as an inexpensive, portable, fast and non-destructive analytical tool to measure colour: Estimation of the ripening stage of tomatoes (*Solanum lycopersicum*) as a case study. *Microchem. J.* **134**, 284–288 (2017).
15. Jiang, W. et al. Ionic liquid-enhanced silica aerogels for the specific extraction and detection of aflatoxin B1 coupled with a smartphone-based colorimetric biosensor. *Food Chem.* **447**, 138917 (2024).
16. Li, S. et al. Smartphone-based reading system integrated with phycocyanin-enhanced latex nanospheres immunoassay for on-site determination of aflatoxin B1 in foodstuffs. *Food Chem.* **360**, 130019 (2021).

17. Apyari, V. et al. Use of household color-recording devices in quantitative chemical analysis. *J. Analyt. Chem.* **72**, 1127–1137 (2017).
18. Rateni, G. et al. Smartphone-based food diagnostic technologies: A review. *Sensors.* **17**(6), 1453 (2017).
19. Hussain, I. et al. Water salinity detection using a smartphone. *Sens. Actuators B: Chem.* **239**, 1042–1050 (2017).
20. Peng, B. et al. A smartphone-based colorimetry after dispersive liquid–liquid microextraction for rapid quantification of calcium in water and food samples. *Microchem. J.* **149**, 104072 (2019).
21. Caleb, J. et al. Smartphone digital image colorimetry combined with solidification of floating organic drop-dispersive liquid-liquid microextraction for the determination of iodate in table salt. *Food Chem.* **336**, 127708 (2021).
22. Razzazi-Fazeli, E. et al. A survey of aflatoxin B1 and total aflatoxin contamination in baby food, peanut and corn products sold at retail in Indonesia analysed by ELISA and HPLC. *Mycotoxin Res.* **20**(2), 51–58 (2004).
23. Yan, H. & Wang, H. Recent development and applications of dispersive liquid–liquid microextraction. *J. Chromatogr. A.* **1295**, 1–15 (2013).
24. Leong, M.-I. et al. Beyond dispersive liquid–liquid microextraction. *J. Chromatogr. A.* **1335**, 2–14 (2014).
25. Lu, L. et al. AFB1 colorimetric aptamer sensor for the detection of AFB1 in ten different kinds of miscellaneous beans based on gold nanoparticles and smartphone imaging. *Food Chem.* **421**, 136205 (2023).
26. Faisal, S. et al. Green synthesis of zinc oxide (ZnO) nanoparticles using aqueous fruit extracts of Myristica fragrans: their characterizations and biological and environmental applications. *ACS Omega.* **6**(14), 9709–9722 (2021).
27. Amirkhizi, B. et al. Aflatoxin B1 in eggs and chicken livers by dispersive liquid–liquid microextraction and HPLC. *Food Addit. & Contam.: Part B.* **8**(4), 245–249 (2015).
28. Khansili, N. et al. Development of colorimetric sensor with zinc oxide nanoparticles for rapid detection of aflatoxin B1 in rice. *Mater. Today: Proc.* **21**, 1846–1855 (2020).
29. Khansili, N. et al. Sensitive metal oxide-clay nanocomposite colorimetric sensor development for aflatoxin detection in foods: Corn and almond. *ACS Omega.* **6**(23), 14911–14925 (2021).
30. Khansili, N. & Krishna, P. M. Curcumin functionalized TiO_2 modified bentonite clay nanostructure for colorimetric Aflatoxin B1 detection in peanut and corn. *Sens. Bio-Sens. Res.* **35**, 100480 (2022).
31. Capitán-Vallvey, L. F. et al. Recent developments in computer vision-based analytical chemistry: A tutorial review. *Analyt. Chim. Acta.* **899**, 23–56 (2015).
32. Moonrungsee, N. et al. Colorimetric analyzer based on mobile phone camera for determination of available phosphorus in soil. *Talanta.* **136**, 204–209 (2015).
33. Amirkhizi, B. et al. Application of the ultrasonic-assisted extraction and dispersive liquid–liquid microextraction for the analysis of AFB1 in egg. *Food Analyt. Methods.* **11**(3), 913–920 (2018).
34. Faisal, S. et al. Fagonia cretica-mediated synthesis of manganese oxide (MnO_2) nanomaterials their characterization and evaluation of their bio-catalytic and enzyme inhibition potential for maintaining flavor and texture in apples. *Catalysts.* **12**(5), 558 (2022).
35. Alikord, M. et al. Biosynthesis of zinc oxide nanoparticles using fermented table olive extract: A novel and green approach with potential applications. *BioNanoScience.* **13**(3), 1036–1051 (2023).
36. Fakhari, S. et al. Green synthesis of zinc oxide nanoparticles: a comparison. *Green Chem. Lett. Rev.* **12**(1), 19–24 (2019).
37. Alkasir, M. et al. Evaluation cytotoxicity effects of biosynthesized zinc oxide nanoparticles using aqueous Linum Usitatissimum extract and investigation of their photocatalytic activityackn. *Inorg. Chem. Commun.* **119**, 108066 (2020).
38. Rai, R. S. et al. An eco-friendly approach on green synthesis, bio-engineering applications, and future outlook of ZnO nanomaterial: A critical review. *Environ. Res.* **221**, 114807 (2023).
39. Rad, S. S. et al. Biosynthesis, characterization and antimicrobial activities of zinc oxide nanoparticles from leaf extract of *Mentha pulegium* (L.). *Microb. Pathog.* **131**, 239–245 (2019).
40. Agarwal, H. et al. A review on green synthesis of zinc oxide nanoparticles–An eco-friendly approach. *Resour.-Effic. Technol.* **3**(4), 406–413 (2017).
41. Burapan, S. et al. Curcuminoid demethylation as an alternative metabolism by human intestinal microbiota. *J. Agric. Food Chem.* **65**(16), 3305–3310 (2017).
42. Porto, I. S., Neto, J. H. S., dos Santos, L. O., Gomes, A. A. & Ferreira, S. L. Determination of ascorbic acid in natural fruit juices using digital image colorimetry. *Microchem. J.* **149**, 104031 (2019).
43. Aydin, I. et al. Development of an accurate and sensitive analytical method for the determination of cadmium at trace levels using dispersive liquid–liquid microextraction based on the solidification of floating organic drops combined with slotted quartz tube flame atomic absorption spectrometry. *J. AOAC Int.* **101**(3), 843–847 (2018).
44. Chen, S. et al. Dispersive liquid–liquid microextraction based on temperature-responsive supramolecular solvent followed by HPLC–DAD for the determination of pyrethroid pesticides in tobacco samples. *Talanta.* **285**, 127350 (2025).
45. Sajid, M. Dispersive liquid-liquid microextraction coupled with derivatization: A review of different modes, applications, and green aspects. *TrAC Trends Analyt. Chem.* **106**, 169–182 (2018).
46. Wang, N. et al. One step rapid dispersive liquid-liquid micro-extraction with in-situ derivatization for determination of aflatoxins in vegetable oils based on high performance liquid chromatography fluorescence detection. *Food Chem.* **287**, 333–337 (2019).
47. Rykowska, I. et al. Modern approaches in dispersive liquid-liquid microextraction (DLLME) based on ionic liquids: A review. *J. Mol. Liq.* **259**, 319–339 (2018).
48. Shi, X. et al. The determination of mycotoxins using isotope-coded labeling and dispersive liquid–liquid microextraction by high throughput flow injection analysis coupled with tandem mass spectrometry. *Microchem. J.* **201**, 110550 (2024).
49. Zgoła-Grześkowiak, A. & Grześkowiak, T. Dispersive liquid–liquid microextraction. *TrAC Trends Analyt. Chem.* **30**(9), 1382–1399 (2011).
50. Herrera-Herrera, A. V. et al. Dispersive liquid–liquid microextraction for determination of organic analytes. *TrAC Trends Analyt. Chem.* **29**(7), 728–751 (2010).
51. Salim, S. A. et al. Dispersive liquid–liquid microextraction (DLLME) and LC–MS/MS analysis for multi-mycotoxin in rice bran: Method development, optimization and validation. *Toxins.* **13**(4), 280 (2021).
52. Jahani, E. et al. In-syringe homogenous liquid–liquid extraction combined with ionic liquid based dispersive liquid–liquid microextraction for the extraction of aflatoxin B1 from edible vegetable oil samples prior to HPLC–FLD analysis. *Microchem. J.* **197**, 109690 (2024).
53. Hamed, A. M. et al. Determination of aflatoxins in plant-based milk and dairy products by dispersive liquid–liquid microextraction and high-performance liquid chromatography with fluorescence detection. *Analyt. Lett.* **52**(2), 363–372 (2019).
54. Zhao, J. et al. Ionic-liquid-based dispersive liquid–liquid microextraction combined with magnetic solid-phase extraction for the determination of aflatoxins B1, B2, G1, and G2 in animal feeds by high-performance liquid chromatography with fluorescence detection. *J. Sep. Sci.* **39**(19), 3789–3797 (2016).
55. Chaisiwamongkhol, K. et al. Smartphone-based colorimetric detection using gold nanoparticles of sibutramine in suspected food supplement products. *Microchem. J.* **158**, 105273 (2020).
56. Solanki, R. et al. Smartphone-based techniques using carbon dot nanomaterials for food safety analysis. *Crit. Rev. Analyt. Chem.* **54**(5), 923–941 (2024).
57. Upadhyay, S. et al. Recent advancements of smartphone-based sensing technology for diagnosis, food safety analysis, and environmental monitoring. *Talanta.* **275**, 126080 (2024).
58. Mulisa, G. et al. Multiple mycotoxin exposure assessment through human biomonitoring in an esophageal cancer case-control study in the Arsi-Bale districts of Oromia region of Ethiopia. *Int. J. Hyg. Environ. Health.* **263**, 114466 (2025).

59. Cheng, Y. et al. Development of a colorimetric/fluorescence dual-mode immunoassay for aflatoxin B1 based on streptavidin-induced gold nanoparticle aggregation. *Microchim. Acta.* **192**(1), 11 (2024).
60. Rubert, J. et al. Application of an HPLC–MS/MS method for mycotoxin analysis in commercial baby foods. *Food Chem.* **133**(1), 176–183 (2012).
61. Bessaire, T. et al. Multiple mycotoxins determination in food by LC-MS/MS: An international collaborative study. *Toxins.* **11**(11), 658 (2019).
62. Wu, L. et al. Development and validation of a DLLME–HPLC–FLD method for determination of aflatoxins in based on quality by design principles. *Phytochem. Anal.* **36**, 1–13 (2024).
63. Khalilipour, G. et al. MOF@N-doped carbon dots-based dispersive solid phase extraction combined dispersive liquid–liquid microextraction of several aflatoxins from raw cow's milk samples prior to HPLC–FLD. *Microchem. J.* **202**, 110806 (2024).
64. Jain, B. et al. A non-instrumental green analytical method based on surfactant-assisted dispersive liquid-liquid microextraction–thin-layer chromatography–smartphone-based digital image colorimetry (SA-DLLME–TLC–SDIC) for determining favipiravir in biological samples. *Molecules.* **28**(2), 529 (2023).
65. Zhao, L. et al. Deep eutectic solvent-based dispersive liquid–liquid microextraction followed by smartphone digital image colorimetry for the determination of carbofuran in water samples. *Analyt. Methods.* **15**(5), 648–654 (2023).
66. Jing, X. et al. Bio-derived solvent-based dispersive liquid-liquid microextraction followed by smartphone digital image colorimetry for the detection of carbofuran in cereals. *J. Food Compos. Anal.* **114**, 104782 (2022).
67. Zhang H, et al. Preparation of aflatoxin B 1 polyclonal antibody and development of an indirect competitive enzyme-linked immunosorbent assay. J Food Agric Environ. **11**, 190–4 (3013).
68. Vdovenko, M. M. et al. Development of ultrasensitive direct chemiluminescent enzyme immunoassay for determination of aflatoxin M1 in milk. *Food Chem.* **158**, 310–314 (2014).
69. Delmulle, B. S. et al. Development of an immunoassay-based lateral flow dipstick for the rapid detection of aflatoxin B1 in pig feed. *J. Agric. Food Chem.* **53**(9), 3364–3368 (2005).
70. Tang, D. et al. Target-induced displacement reaction accompanying cargo release from magnetic mesoporous silica nanocontainers for fluorescence immunoassay. *Anal Chem.* **85**(21), 10589–10596 (2013).
71. Wang, Y. et al. Simultaneous and rapid detection of six different mycotoxins using an immunochip. *Biosens. Bioelectron.* **34**(1), 44–50 (2012).
72. Xu, G. et al. Magnetic functionalized electrospun nanofibers for magnetically controlled ultrasensitive label-free electrochemiluminescent immune detection of aflatoxin B1. *Sens. Actuators B: Chem.* **222**, 707–713 (2016).
73. Tang, X. et al. Colorimetric detection of Aflatoxin B1 by using smartphone-assisted microfluidic paper-based analytical devices. *Food Control.* **132**, 108497 (2022).
74. Wang, X. Magnetic bead-based immunoassays for aflatoxin B1 using biofunctionalized gold nanoparticles: Technische Universität München. *Sensors (Basel)* **14**(11), 21535–21548. https://doi.org/10.3390/s141121535 (2014).

Author contributions

Mahsa Alikord and Nabi Shariatifar: Supervision, Project administration, writing—review & editing, Writing—original draft, Formal analysis, Validation, Software, Data curation and Funding acquisition. Mammad Saraji: Methodology, Formal analysis, Data curation, Validation, Software. Hedayat Hosseini, Gholamreza Jahed Khaniki, Shahram Shoeibi and Toba Rezazadeh and Mohammad Fazeli: Conceptualization, Investigation, Methodology, Formal analysis, Data curation.

Funding

This project was supported by a grant from the Tehran University of Medical Sciences as a Ph.D. thesis (Grant Number: 51033, Ethics Code: IR.TUMS.SPH.REC.1399.304). This work is based upon research funded by Iran National Science Foundation (INSF) (N = 4040708).

Declarations

Competing interests

The authors declare no competing interests.

Additional information

Supplementary Information The online version contains supplementary material available at https://doi.org/10.1038/s41598-025-92944-3.

Correspondence and requests for materials should be addressed to M.A. or N.S.